DOI: 10.1002/cphc.201200900

Mechanism of Framework Oxygen Exchange in Fe-Zeolites: A Combined DFT and Mass Spectrometry Study

Prokopis C. Andrikopoulos, Zdenek Sobalik, Jana Novakova, Petr Sazama, and Stepan Sklenak*[a]

The role of framework oxygen atoms in N_2O decomposition [$N_2O(g) \rightarrow N_2(g)$ and $^1/_2O_2(g)$] over Fe-ferrierite is investigated employing a combined experimental ($N_2{}^{18}O$ decomposition in batch experiments followed by mass spectroscopy measurements) and theoretical (density functional theory calculations) approach. The occurrence of the isotope exchange indicates that framework oxygen atoms are involved in the N_2O decomposition catalyzed by Fe-ferrierite. Our study, using an Fe-ferrierite sample with iron exclusively present as Fe^{II} cations accommodated in the cationic sites, shows that the mobility of framework oxygen atoms in the temperature range: 553 to 593 K is limited to the four framework oxygen atoms of the two AlO_4^- tetrahedra forming cationic sites that accomodate Fe^{II}. They exchange with the Fe extra-framework ^{18}O atom originating from the decomposed $N_2{}^{18}O$. We found, using DFT calculations, that O_2 molecules facilitate the oxygen exchange. However, the corresponding calculated energy barrier of 87 kcal mol^{-1} is still very high and it is higher than the assumed experimental value based on the occurrence of the sluggish oxygen exchange at 553 K.

1. Introduction

Silicon-rich zeolites (Si/Al > 8), such as ZSM-5 (MFI), mordenite (MOR), ferrierite (FER) and beta (*BEA) zeolites represent catalytic materials with wide industrial application. Their transition-metal-exchanged forms were discovered as exceptional redox catalysts.[1] Fe-zeolites together with Cu-zeolites are the two most important systems as they have real potential for applications in industrial processes under real conditions. Fe-zeolites were studied as catalysts for a spectrum of related environmental processes, such as N_2O decomposition,[2] N_2O selective oxidation,[3] N_2O selective catalytic reduction (SCR),[2c] direct NO decomposition,[2g] as well as for SCR of NO_x using various reducing agents.[2g,4]

A direct relationship between the parameters of the N_2O decomposition and an isotope exchange of O_2 and O atoms present in oxide catalysts was established by Winter decades ago.[5] Later, the role of framework oxygen atoms in the decomposition of nitrous oxide was also investigated over zeolites containing metal cations.[2a,6] Leglise et al.[6a] studied the decomposition of $N_2{}^{16}O$ over exhaustively ^{18}O-oxygenated Fe-FAU (FAU: faujasite) and Fe-MOR zeolites and detected ^{18}O in the oxygen molecules in the gas phase, thus showing an involvement of framework oxygen atoms in the decomposition. Valyon et al.[6b] employed nitrous oxide labeled by ^{18}O in the reaction over Fe-MOR at 673 K and learned that the isotope exchange included framework oxygens. They assumed that there were two “portholes” in the catalysts, one for the entrance of oxygen from decomposing N_2O, and the other for the exit of a different oxygen atom from the catalyst. The mobility of framework oxygen atoms of Fe-MFI was suggested by Pirngruber et al.[6c,d] to explain the appearance of ^{18}O labeled oxygen during an experiment similar to Leglise et al.,[6a] that is, the interaction of $N_2{}^{16}O$ with ^{18}O enriched catalysts. However, due to the high concentration of various Fe oxidic species present in their samples, we assume that part of the exchanged oxygen atoms could originate from the oxidic Fe species (see ref. [5b]). Panov et al.[2a] investigated highly active oxygen atoms formed in Fe-MFI during the decomposition of nitrous oxide. They concluded that the isotope exchange between $^{18}O_2$ and the active oxygen proceeds with a minor activation energy and that the equilibration of O_2 isotopologues without direct involvement of the active oxygen occurs even at cryogenic temperatures.[6e,k] Sobalik et al. observed: 1) a room-temperature isotope exchange of $^{18}O_2$ with Fe extra-framework ^{16}O of Fe-FER oxidized by $N_2{}^{16}O$, and 2) the involvement of framework oxygen atoms in experiments with $N_2{}^{18}O$ in the production of O_2.[6f,g]

In the present study, we investigated the role of Fe framework oxygen atoms of Fe-ferrierite in the $N_2{}^{18}O$ decomposition over the catalyst with a very low iron content and thus a negligible amount of iron oxides. This isotope exchange is the only source of ^{16}O in the O_2 molecules formed by the $N_2{}^{18}O$ decomposition. All O_2 molecules originate from decomposed $N_2{}^{18}O$ as there is no O_2 added. The exception is the experiment with a mixture of $^{18}O_2$ and $^{16}O_2$ without the presence of N_2O. We carried out the $N_2{}^{18}O$ decomposition over Fe-ferrierite in batch experiments which were followed by mass spectroscopy measurements. In addition, we employed periodic density functional

---

[a] Dr. P. C. Andrikopoulos, Dr. Z. Sobalik, Dr. J. Novakova, Dr. P. Sazama, Dr. S. Sklenak
J. Heyrovský Institute of Physical Chemistry
of the Academy of Sciences of the Czech Republic
Dolejškova 3, 182 23 Prague 8 (Czech Republic)
E-mail: stepan.sklenak@jh-inst.cas.cz

Supporting information for this article is available on the WWW under http://dx.doi.org/10.1002/cphc.201200900.

© 2013 Wiley-VCH Verlag GmbH & Co. KGaA, Weinheim

theory (DFT) calculations to examine the mechanisms of the isotope exchange.

Our model considers the Fe^{II} exchanged ferrierite without structural defects, with Fe^{II} accommodated exclusively in the α and β cationic sites, and without the presence of oxidic Fe species.[2e,7] Also, within the scope of this study is the correlation with experiments at a low N_2O pressure, so as to limit the involvement of atoms other than oxygen and iron. Investigation of the mechanism of the isotope exchange in the high-temperature region when most framework oxygen atoms can be potentially involved in the exchange is beyond the scope of this study.

Experimental and Computational Methods

Ferrierite Samples

Fe-FER: Na,K-FER (Tosoh, Japan; Si/Al 8.6) was used as the parent zeolite to prepare Fe-FER. The parent was the same as that used in our prior studies.[2e,7] The $Fe_{0.04}$-FER sample (0.04 is the Fe/Al ratio) was prepared using the procedure based on an impregnation of the parent ammonia zeolite form by a $FeCl_3$ solution in acetyl-acetone, followed by a calcination in an air stream at 700 K for 10 h. The procedure is described in detail elsewhere.[8] The Fe/Al ratio of the $Fe_{0.04}$-FER sample was very low, significantly below the maximum ion-exchange capacity for Me(II) cations which is 0.33,[9] to guarantee the exclusive presence of cationic Fe^{II} accommodated in the α and β sites in the sample.[2h,10] In addition, EPR spectroscopy confirmed the absence of Fe^{III} in the Fe-FER sample used.[10] The heating of the $Fe_{0.04}$ sample up to 700 K led to no release of O_2. Our prior study showed that O_2 is evolved only from Fe-FER samples with a significantly higher Fe/Al ratio (Fe/Al 0.26) during heating.[2e]

H-FER: H-FER was provided by Vyzkumny ustav anorganicke chemie, a.s., Czech Republic. The sample, which was synthesized from extra-pure components and exchanged into H-FER via the ammonium form, contains less than 50 ppm of Fe and therefore it was used for comparison.

represent the corrected MS signals showing a value of 1.0 for the initial amount of N_2O.

Studied Reactions

The role of the Fe-framework oxygen atoms, hereafter designated by O_{FR} [i.e. the four oxygen atoms of the two AlO_4^- tetrahedra located in the six-membered rings forming the cationic sites for the divalent cations $Fe((^{16}O_{FR})_4)$-FER[7]] of Fe-ferrierite in the $N_2{}^{18}O$ decomposition is studied [Eq. (1)]:

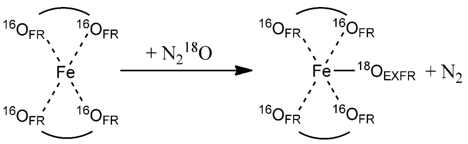

(1)

$N_2{}^{18}O$ oxidizes the Fe^{II} cation accommodated in a cationic position of ferrierite to yield $^{18}O{=}Fe((^{16}O_{FR})_4)$-FER and N_2(g). Then, the extra-framework ^{18}O atom, hereafter designated O_{EXFR}, can exchange with O_{FR} atoms to give $^{16}O_{EXFR}{=}Fe((^{16}O_{FR})_3{}^{18}O_{FR})$-FER [Eq. (2)]:

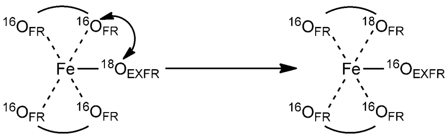

(2)

There is another isotope exchange which occurs in the studied catalyst. It is the isotope exchange of O_{EXFR} with O_2(g) molecules [O_2 originating from decomposed N_2O or eventually added O_2 (not our study)]. This process is responsible for the equilibration of the isotopologues of the O_2 molecules [Eq. (3)]:

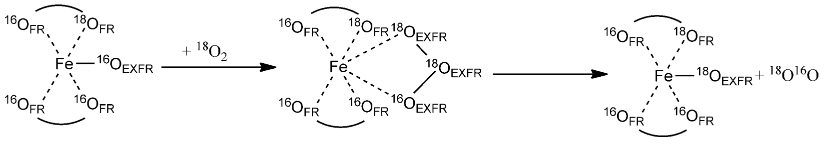

(3)

Measurements in the Batch Reactor

About 100 mg of the ferrierite samples described above were placed in a glass reactor (reaction volume of 287 cm^3). The samples were pretreated in situ in vacuum at 700 K prior to exposure to $^{15}N_2{}^{18}O$ at about 180 Pa (Medical Isotopes Inc., USA, 99 % of ^{18}O; the double labeled compound was used, but the nitrogen isotope does not play any role in the reactions; therefore the $N_2{}^{18}O$ formula is used in the text). A simple equilibration between oxygen molecules without the presence of N_2O was measured using an equimolecular mixture of $^{16}O_2$ and $^{18}O_2$. The progress of the N_2O decomposition and that of the isotope composition was monitored using a Balzers QMG 420 quadrupole mass spectrometer. A negligible amount of the gas phase was continuously fed into the analytic chamber of the mass spectrometer via a needle valve. Pure compounds, including all the isotope combinations, were employed for the calibration. The mass spectrometry (MS) signals were converted to the amounts of the individual compounds using calibration and corrections for fragmentation. For brevity, the Y axes in the figures

We employed periodic DFT calculations to examine the mechanisms, including all the transition states and intermediates, responsible for the two isotope exchanges [Eqs. (2) and (3)]. Eqs. (1)–(3) are schematic because they show only the active site of Fe-ferrierite. However, our periodic DFT computations use the entire super cell of Fe-ferrierite composed of one or two unit cells depending on the structural model.

Structural Models

Herein, we used four models of Fe-ferrierite which are the same as those employed in our previous study.[7] The four models, possessing P1 symmetry, were utilized to investigate four distinct possible arrangements of the active sites in ferrierite. The first two models (α and β−2) represent isolated cationic sites while the other two models (β−1+β−1 and β−2+β−2) feature two cooperating adjacent Fe^{II} cationic sites. The β−1 model was not used in this study since N_2O does not adsorb via the O atom on Fe^{II} accommodated

© 2013 Wiley-VCH Verlag GmbH & Co. KGaA, Weinheim

in isolated β−1 sites,[7] and therefore, no isotope exchange can occur. Moreover, our recent study[9] of the parent ferrierite zeolite (FER/D in ref. [9]) revealed that β−2 and α cationic sites are present in the sample. The optimized structures of molecular dynamics simulations obtained in our prior study[7] were employed as the starting structures.

Electronic Structure Calculations

Spin-polarized periodic DFT calculations were carried out employing the VASP code.[11] The high-spin configuration Fe $d^5\uparrow\ d^1\downarrow$[12] and other possible spin states were employed for all the minima and transition states to localize the electronic ground state for all the species. The Kohn–Sham equations were solved variationally in a plane-wave basis set using the projector-augmented wave (PAW) method of Blöchl,[13] as adapted by Kresse and Joubert.[14] The exchange–correlation energy was described by the PW91 generalized gradient approximation (GGA) functional.[15] Brillouin zone sampling was restricted to the Γ-point. A plane-wave cutoff of 400 eV was used.

Electronic structure calculations do not consider nuclei of different isotopes and therefore all isotope-exchange reactions are thermoneutral as the reactants and products are chemically identical.

Geometry Optimizations

The atomic positions were optimized by employing a conjugate-gradient algorithm minimization of energies and forces while the lattice parameters were fixed (constant volume) at their experimental values. Transition structures were identified using the dimer method,[16] as recently improved by Heyden et al.[17]

2. Experimental Results

2.1. Concentration of ^{18}O in the Released O_2 Molecules and the Q Variable

The concentration of ^{18}O (in %) in the released O_2 molecules originating from the decomposing $N_2{}^{18}O$ is given by Equation (4):

$$\%^{18}\mathrm{O} = \frac{100 \times ([^{16}\mathrm{O}^{18}\mathrm{O}] \times 0.5 + [^{18}\mathrm{O}^{18}\mathrm{O}])}{[^{16}\mathrm{O}^{16}\mathrm{O}] + [^{16}\mathrm{O}^{18}\mathrm{O}] + [^{18}\mathrm{O}^{18}\mathrm{O}]} \quad (4)$$

The concentration of ^{18}O serves as a measure of the isotope exchange between O_{EXFR} and O_{FR}.

The *Q* variable is defined as [Eq. (5)]:

$$Q = [^{16}\mathrm{O}^{18}\mathrm{O}]^2/([^{16}\mathrm{O}^{16}\mathrm{O}] \times [^{18}\mathrm{O}^{18}\mathrm{O}]) \quad (5)$$

The *Q* variable presents a measure of the equilibrium among the isotopologues of O_2 molecules and attains the value of four when the equilibrium is reached.[18]

2.2. $N_2{}^{18}O$ Decomposition

The decomposition of $N_2{}^{18}O$ over H-FER at 673 K is nearly negligible (see Figure S1 of the Supporting Information, SI) while that over Fe-FER occurs above 493 K[6f] and proceeds with increasing rate at 553, 573, and 593 K (Figure 1). The equilibration of oxygen isotopologues released into the gas phase occurs at all three temperatures. The concentration of ^{18}O reaches about 55 % at 553 K, 50 % at 573, and 45 % at 593 K and the *Q* variable is equal to four for all the temperatures (Figure 1).

Table 1 shows the ratios of the number of ^{18}O exchanged to the number of Fe cations (O_{exch}/Fe) as well as of the number of $N_2{}^{18}O$ decomposed to the number of Fe cations (N_2O_{decomp}/Fe) in $Fe_{0.04}$-FER after 40 min of the N_2O decomposition for the temperatures in the interval from 553 to 593 K. The O_{exch}/Fe and N_2O_{decomp}/Fe ratio values range from 0.7 and 1.6 at 553 K to 1.4 and 2.9 at 593 K, respectively. Both the O_{exch}/Fe and N_2O_{decomp}/Fe ratio values increase as the temperature rises, but the O_{exch}/Fe values do not exceed 4, which is consistent with the number of O_{FR} forming the cationic site.

Table 1. Ratios of the number of ^{18}O exchanged to the number of Fe cations (O_{exch}/Fe) and of the number of $N_2{}^{18}O$ decomposed to the number of Fe cations (N_2O_{decomp}/Fe) in $Fe_{0.04}$-FER after 40 min of N_2O decomposition at various temperatures (in K).

Temperature	O_{exch}/Fe	N_2O_{decomp}/Fe
553	0.7	1.6
573	1.1	2.6
593	1.4	2.9

The equilibration of a mixture of $^{18}O_2$ and $^{16}O_2$ without the presence of N_2O (i.e. in the absence of O_{EXFR}) does not occur and the isotope composition remains constant during the time of the experiment (not shown in the figures).

3. Computational Results

3.1. Spin States

The high-spin configuration Fe $d^5\uparrow\ d^1\downarrow$ was found to be the electronic state for all the species calculated allowing for a complete potential energy surface, where all minima and transitions states are calculated, and leading to the lowest energy barriers (see Table S1). In this configuration, the structures with one Fe have four unpaired electrons in total while those with two Fe have eight unpaired electrons. The exceptions are complexes **2**′ and **4**′ (Scheme 1) as well as the very weak monodentate complexes **7**′ and **9**′ (Scheme 2) in which the O_2 moiety only loosely interacts with the active site. The **7**′ and **9**′ complexes have six unpaired electrons, four of which are located on Fe and two on the O_2 moiety. Spin-state changes throughout the course of the reaction for systems containing transition metals are quite common.[19]

3.2. Mechanism of the Isotope Exchange

Four different mechanisms were computationally investigated to explain our experimental findings. The former two correspond to Equation (3), while the latter two to Equation (2). Specifically, we report the results for the isotope exchange be-

© 2013 Wiley-VCH Verlag GmbH & Co. KGaA, Weinheim

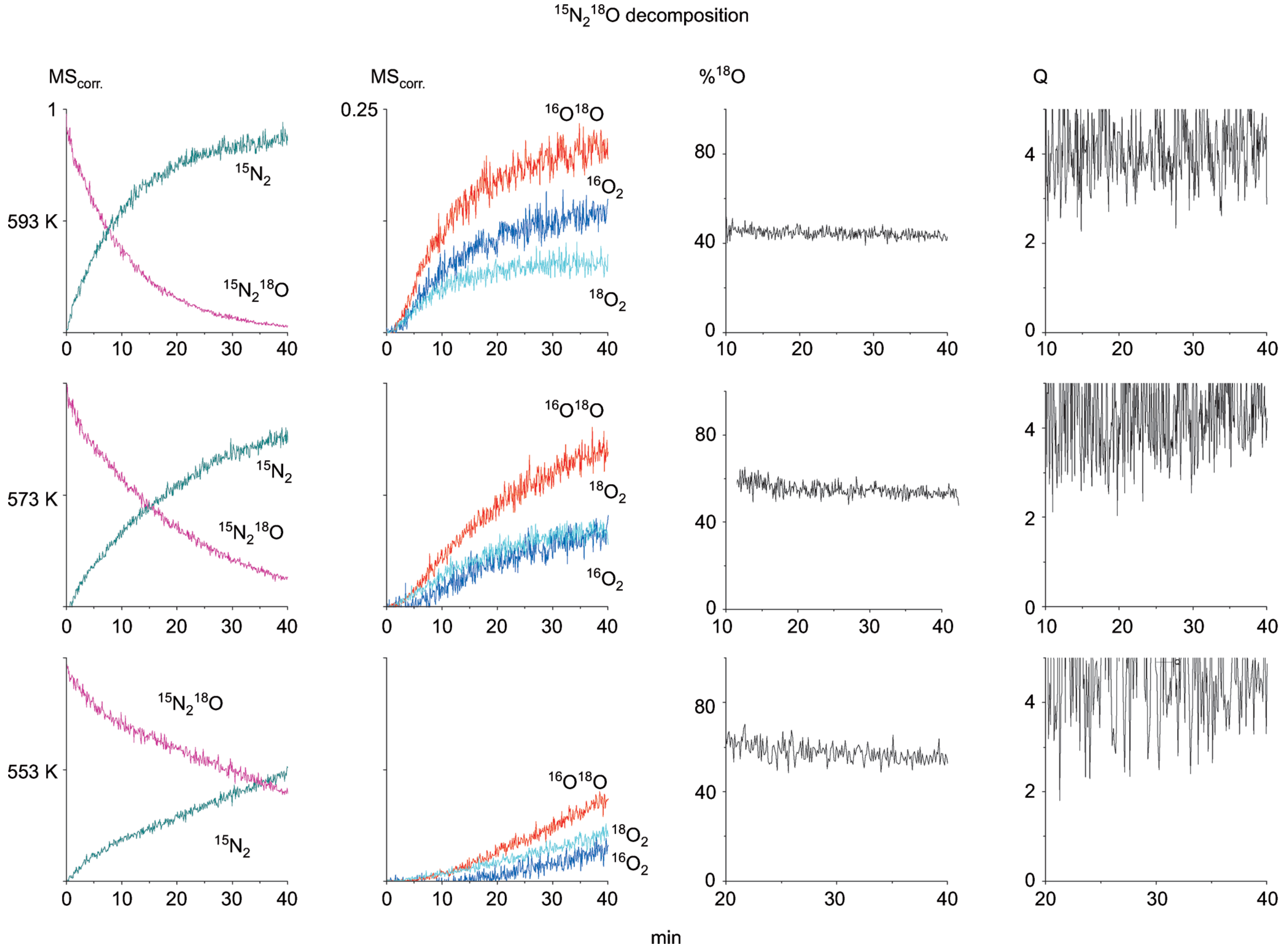

Figure 1. Temperature effect (temperature in K) on the decomposition of nitrous oxide over $Fe_{0.04}$-FER. The weight of the sample was 109 mg; the initial pressure of $N_2{}^{18}O$ was 179 Pa. The corrected MS signals ($MS_{corr.}$), showing the amount of $N_2{}^{18}O$, N_2, ${}^{18}O_2$, ${}^{18}O{}^{16}O$, and ${}^{16}O_2$ during the decomposition of $N_2{}^{18}O$ and formation of N_2 and O_2 isotopologues, are presented. The corrected MS value is 1.0 for the initial amount of N_2O equal to 22 μmol of N_2O. For brevity, the *y* axes in the figures represent % of ${}^{18}O$ in oxygen isotopologues, and *Q*.

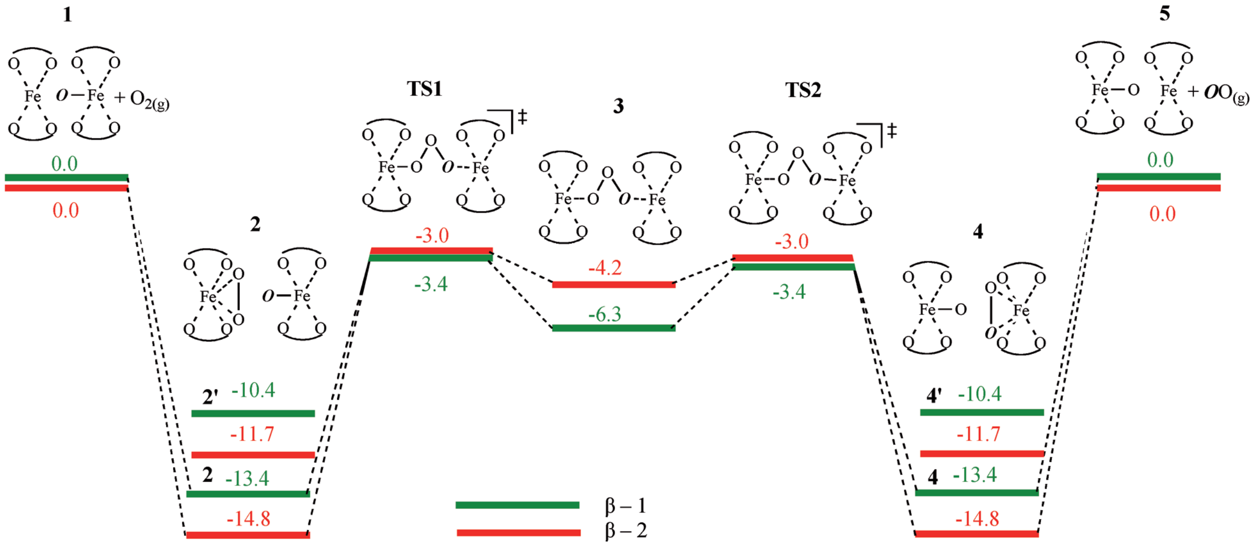

Scheme 1. Schematic energy profiles (in kcal mol^{-1}) for the isotope exchange between O_{EXFR} atoms and O_2 molecules occurring on two Fe^{II} cations accommodated in two adjacent β−1 and β−2 sites. ***O*** is ${}^{18}O$ originating from $N_2{}^{18}O$. Complexes **2′** and **4′** have ten unpaired electrons while all the other species have eight. The energy profiles for both sites are independent and are not interconnected.

© 2013 Wiley-VCH Verlag GmbH & Co. KGaA, Weinheim

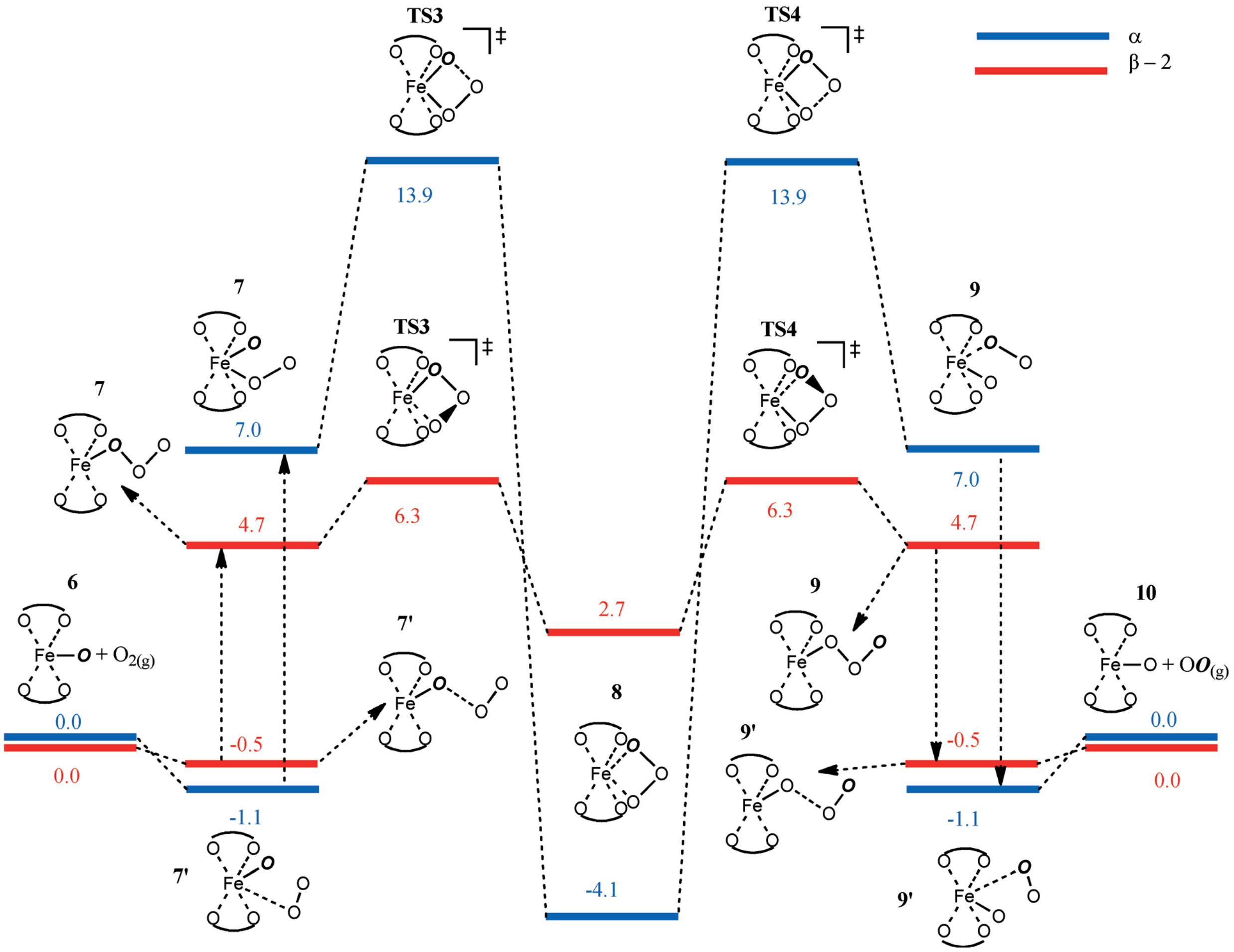

Scheme 2. Schematic energy profiles (in kcal mol^{-1}) for the isotope exchange between O_{EXFR} atoms and O_2 molecules proceeding on Fe^{II} located in an isolated α and β–2 cationic site. ***O*** is ^{18}O originating from $N_2{}^{18}O$. Complexes **7**′ and **9**′ have six unpaired electrons while all the other species have four. The energy profiles for both sites are independent and are not interconnected.

tween O_{EXFR} and O_2 molecules occurring on the active site composed of two collaborating Fe^{II} cations (Section 3.2.1; Scheme 1) as well as on isolated Fe^{II} cations (Section 3.2.2; Scheme 2). The mechanism introduced in Section 3.2.3 (Scheme 3) examines the isotope exchange between $^{18}O_{EXFR}$ and $^{16}O_{FR}$. This process involves framework oxygen atoms and is only considered for isolated Fe^{II} sites since no benefit can be gained from a bimetallic active site, due to the large distance between the two Fe^{II} cations. Scheme 3 reveals that the energy cost of a creation of an oxygen vacancy starting from the ferrierite framework without structural defects is prohibitively high. Therefore, other possible processes were investigated to rationalize the framework oxygen mobility. This resulted into a discovery of another mechanism of the isotope exchange between $^{18}O_{EXFR}$ and $^{16}O_{FR}$ which involves O_2 molecules. This mechanism which corresponds to the more facile exchange is described in Section 3.2.4 (Scheme 4).

3.2.1. Mechanism of the Isotope Exchange between O_{EXFR} and O_2 Molecules on the Active Sites Composed of Two Collaborating Fe^{II} Cations

We reported in our previous study that two Fe^{II} cations coordinated in two adjacent β sites of Fe-ferrierite most likely form the active site responsible for the superior activity of Fe-ferrierite in the N_2O decomposition over Fe-ZSM-5 and Fe-beta in the low-temperature region.[7] Naturally, we also tested this type of active site for the oxygen-exchange mechanism.

Scheme 1 reveals the reaction mechanism of the isotope exchange between $^{18}O_{EXFR}$ and an $^{16}O_2$ molecule occurring on two Fe^{II} cations accommodated in two adjacent β sites. $N_2{}^{18}O$ oxidizes the Fe(1) cation to form complex **1** (Figure S2 of the SI).[7] Then, $^{16}O_2$ adsorbs on Fe(2) to form complex **2** (Figure S3 of the SI). The calculations on the β–1+β–1 and β–2+β–2 models yield adsorption energies of –13.4 and –14.8 kcal mol^{-1} for the β–1 and β–2 sites, respectively. Complex **2** has eight unpaired electrons and the O_2 moiety is in a singlet state. The spin variant of complex **2** with ten unpaired electrons (complex **2**′) is higher in energy by 3.0 and 3.1 kcal mol^{-1} for the β–1 and β–2 sites, respectively, but it is more stable

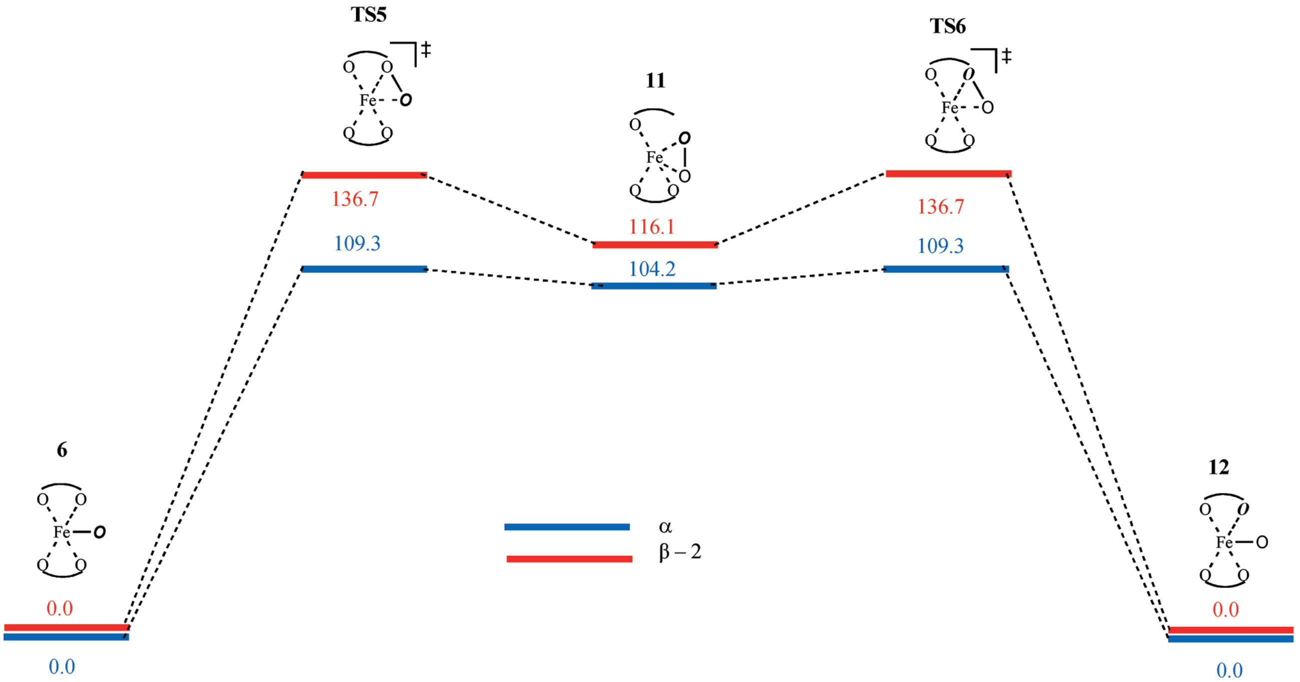

Scheme 3. Schematic energy profiles (in kcal mol^{-1}) for the isotope exchange between O_{EXFR} atoms and O_{FR} atoms in the absence of O_2 molecules occurring on Fe^{II} located in an isolated α and β–2 cationic site. ***O*** is ^{18}O originating from $N_2{}^{18}O$. The energy profiles for both sites are independent and are not interconnected.

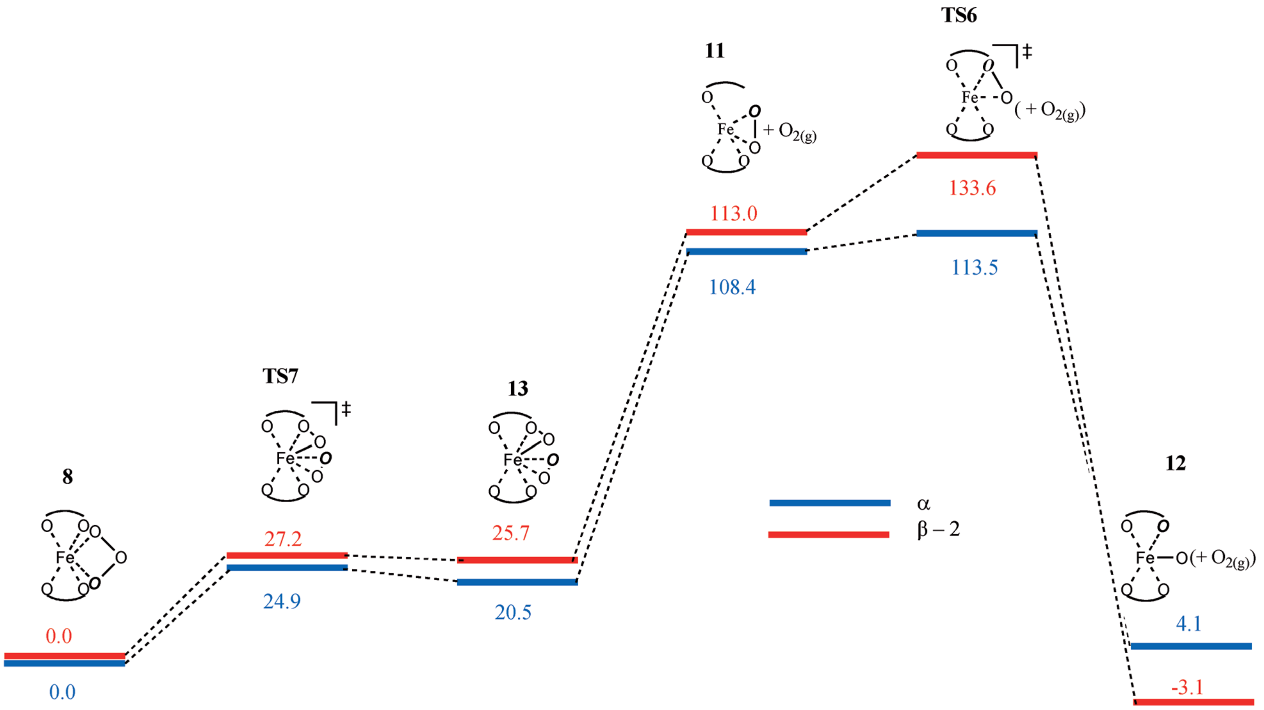

Scheme 4. Schematic energy profiles (in kcal mol^{-1}) for the isotope exchange between O_{EXFR} atoms and O_{FR} atoms in the presence of O_2 molecules occurring on Fe^{II} located in an isolated α and β–2 cationic site. ***O*** is ^{18}O originating from $N_2{}^{18}O$. The energy profiles for both sites are independent and are not interconnected. The energy of O_2(g) is added to the energy of the species **11**, **TS6**, and **12** to maintain the same number of atoms for all the species.

than complex **1** and the O_2(g) is in a triplet state (Scheme 1). Our scan calculations (i.e. computations of a series of points along the reaction coordinate) reveal that when an O_2(g) molecule in a triplet state approaches Fe^{II} of complex **1** then the energy drops monotonously till complex **2′** is formed. However, as O_2 gets closer to Fe^{II} of complex **1**, then the spin variant with eight unpaired electrons becomes more stable than that with ten unpaired electrons. A spin change can occur at this point and the energy further monotonously decreases as complex **2** is yielded (not shown in the figures). It is obvious from these calculations that the formation of complex **2** is barrierless.

The two adsorbed ^{16}O atoms rearrange to form a ^{16}O–^{18}O bond with the ^{18}O atom to yield complex **3** (Figure S4 of the SI) with a –^{16}O–^{16}O–^{18}O– fragment bound to both of the Fe^{II} cations via transition state **TS1** (Figure S5 of the SI). This reaction step is endothermic as the corresponding reaction energies are 7.1 and 10.6 kcal mol^{-1} for the β−1 and β−2 sites, respectively. The exchange is fast as the calculated barriers are only 10.0 and 11.8 kcal mol^{-1} for the β−1 and β−2 sites, respectively. The ^{16}O–^{16}O bond of the –^{16}O–^{16}O–^{18}O– fragment in complex **3** is instantly cleaved (the corresponding barriers have negligible values of 2.9 and 1.2 kcal mol^{-1} for the β−1 and β−2 sites, respectively) and complex **4** is formed (the reaction energies are −7.1 and −10.6 kcal mol^{-1} for the β−1 and β−2 sites, respectively) via transition state **TS2** (Scheme 1). Subsequently, an $^{18}O^{16}O$ molecule desorbs from Fe^{II} to the gas phase. The formation of complex **3** is calculated to be the rate-determining step of the isotope exchange between $\mathbf{O}_{EXFR}$ and an O_2 molecule occurring on two Fe^{II} cations accommodated in two adjacent β sites.

3.2.2. *Mechanism of the Isotope Exchange between O_{EXFR} and O_2 Molecules on the Active Sites Composed of Isolated Fe^{II} Cations*

The mechanism of the isotope exchange between O_{EXFR} and the O_2 molecule differs on Fe^{II} located in an isolated cationic site (the α and β−2 models; Scheme 2). The structure of the cationic sites accommodating oxidized iron cations (complex **6** in Scheme 2) is depicted in Figure S6 of the SI. Fe^{II} accommodated in isolated α and β−2 sites is oxidized by $N_2{}^{18}O$ to form the Fe–^{18}O complex (complex **6** in Scheme 2) via the Fe···^{18}ONN complex.[7] Fe^{II} coordinated in an isolated β−1 site cannot be oxidized in this way since the Fe···ONN complex is not formed.[7]

$^{16}O_2$ in a triplet state interacts with the Fe-^{18}O complex to give the very weak complex **7′**. The interaction energies are only −1.1 and −0.5 kcal mol^{-1} for the α and β−2 sites, respectively. The loosely coordinated O_2 moiety of complex **7′** has two unpaired electrons and there are four more on Fe, thus complex **7′** has six unpaired electrons in total. The structure of **7′** significantly differs for the α and β−2 sites. One of the oxygen atoms of O_2 is weakly ligated to the Fe^{II} atom (Fe···O distance is 3.088 Å) for the α site, while for the β−2 site the closest contact is to the O_{EXFR} atom (O_{EXF}···O distance is 2.357 Å).

In order for the oxygen exchange to proceed, a spin change of the weakly adsorbed O_2 from triplet to singlet must occur. This is accompanied by a shortening of the Fe···O (α site) and O–O (β−2 site) distance to 2.139 and 1.592 Å, respectively, to yield complex **7** (Figure 2). Complex **7** has a total of four unpaired electrons, and is calculated to be less stable than **7′** by 8.1 and 5.2 kcal mol^{-1} for the α and β−2 sites, respectively.

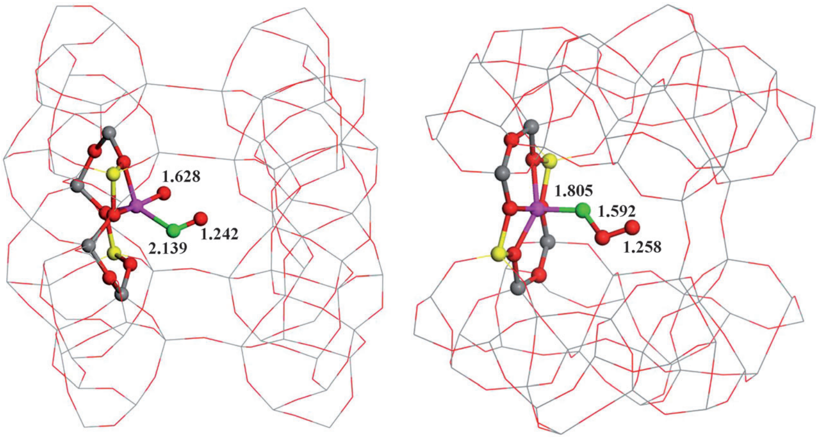

Figure 2. Optimized structure of complex **7** [α model (left) and β−2 model (right)]. The distances are in Å. Silicon atoms are in gray, aluminum atoms in yellow, iron atoms in violet, and oxygen atoms in red; the O_{EXFR} atom is shown in green.

Our calculations reveal that when the distance between the O atom of the O_2 moiety which is weakly ligated to either: 1) the Fe^{II} atom (α site) or 2) the O_{EXFR} atom (β−2 site) decreases beyond the equilibrium distance in complex **7′** (3.088 and 2.357 Å, respectively), the energy of the spin variant with six unpaired electrons increases. Furthermore, when the same bond increases from its equilibrium value in complex **7** (2.139 and 1.592 Å), the energy of the calculated system of the spin variant with four unpaired electrons increases. The spin change occurs at the point at which the two energy curves cross each other. The difference between the energy of the curve crossing and the energies of 7 and 7′ corresponds to the barriers for the 7→7′ and 7′→7 processes, respectively. The numerical noise prevented us from calculating smooth energy curves to accurately determine the barriers for 7→7′ and 7′→7. Instead, we used a published barrier for a similar system. Berthomieu et al. studied the formation of molecular oxygen on the $[Fe(\mu\text{-}O)(\mu\text{-}OH)Fe]^{+}$ site of the ZSM-5 zeolite.[20] They obtained a spin change barrier of 14.6 kcal mol^{-1} for a change of adsorbed O_2 from triplet to singlet using a method to locate the MECP (minimum energy crossing point).[21] We assume that this value could be a rough estimate of the barrier for 7′→7.

The formation of complex **8** differs for the two active sites. The oxygen atom of the O_2 moiety of **7** (α site) which is not coordinated to Fe forms a bond with $^{18}O_{EXFR}$ to give complex **8** with a –^{16}O–^{16}O–^{18}O– ring (Figure 3) via **TS3** (Figure S7 of the SI) (the reaction energy is −11.1 kcal mol^{-1} and the barrier is 6.9 kcal mol^{-1}). Subsequently the ^{16}O–^{16}O bond in the –^{16}O–^{16}O–^{18}O– fragment of complex **8** breaks to yield complex **9** via

© 2013 Wiley-VCH Verlag GmbH & Co. KGaA, Weinheim

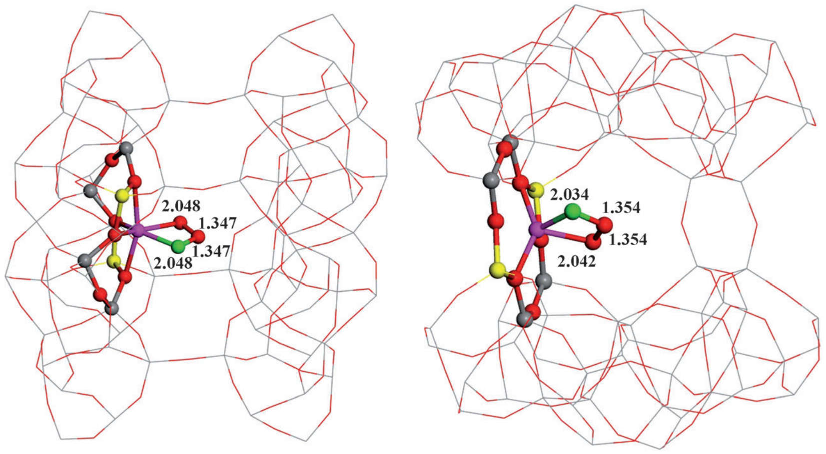

Figure 3. Optimized structure of complex **8** [α model (left) and β−2 model (right)]. The distances are in Å. Silicon atoms are in gray, aluminum atoms in yellow, iron atoms in violet, and oxygen atoms in red; the O_{EXFR} atom is shown in green.

transition state **TS4** (the reaction energy is 11.1 kcal mol^{-1} and the barrier is 18.0 kcal mol^{-1}). On the other hand, for the β−2 site, the $-^{16}O-^{16}O-^{18}O-$ fragment of **7** rotates to yield complex **8** with a $-^{16}O-^{16}O-^{18}O-$ ring (Figure 3) via **TS3** (Figure S7 of the SI). This reaction step is exothermic by −2.0 kcal mol^{-1} and very fast with a very small barrier of 1.6 kcal mol^{-1}. Similarly, **8** can change via **TS4** to **9** by a rotation of the $-^{16}O-^{16}O-^{18}O-$ fragment (the reaction energy is 2.0 kcal mol^{-1} and the barrier is 3.6 kcal mol^{-1}).

Complex **9** undergoes a spin crossover to give **9′** with six unpaired electrons, two of them are located on the O_2 moiety while four are on Fe. The $^{18}O^{16}O$ molecule resulting from the previous reaction step can desorb to the gas phase. Species **7**, **TS3**, **8**, **TS4**, and **9** have four unpaired electrons and lie on one potential energy surface. The cleavage of the $^{16}O-^{16}O$ bond in complex **8** to give complex **9** is calculated to be the rate-determining step of the isotope exchange on isolated Fe^{II} cations in the α site. On the other hand, the spin change 7′→7 is most likely the rate-determining step for the exchange on isolated Fe^{II} cations located in the β−2 site, because all the corresponding barriers are very small. It should be stressed here that the different pathways followed by the α and β−2 sites in this scheme were dictated by the structural features of their respective weak complexes (**7′**). Other than those reported, all attempts to locate other weak complexes between O_2 and O_{EXFR} or Fe were unsuccessful. Therefore, we can conclude that most likely there is no low barrier pathway for the isotope exchange on isolated Fe^{II} cations in the α site analogous to that on the isolated Fe^{II} coordinated in the β−2 site.

The isotope exchange between O_{EXFR} and O_2 atoms occurring on Fe^{II} located in an isolated α site is more sluggish than that proceeding on two cooperating Fe^{II} cations, as the largest barrier for the former is 18 kcal mol^{-1}, while for the latter the highest barriers are 10 and 12 kcal mol^{-1} for the β−1 and β−2 sites, respectively. On the other hand, the rate of exchange on Fe^{II} positioned in an isolated β−2 site is most likely comparable with that on two collaborating Fe^{II} cations since the spin change 7′→7 is most likely the slowest step of the exchange.

3.2.3. Mechanism of the Isotope Exchange between O_{EXFR} and O_{FR} in the Absence of O_2 Molecules

The isotope exchange between O_{EXFR} and O_{FR} cannot benefit from the proximity of the two Fe^{II} cations accommodated in two adjacent β sites because the distance between O_{EXFR} and the other Fe^{II} cation is 5.3 Å. Therefore, we investigated this exchange only using two models of isolated cationic sites (the α and β−2 models).

Our DFT simulations reveal that O_2 molecules play an important role in the isotope exchange between O_{EXFR} and O_{FR} (see Section 3.2.4). Since there is no O_2 present in the initial stage of the $N_2{}^{18}O$ decomposition, our computations reveal (Scheme 3) that the isotope exchange proceeds directly via complex **11** (Figure 4) and transition state **TS5** (Figure 5). One of the four $^{16}O_{FR}$ atoms and the $^{18}O_{EXFR}$ atom approach each other and their distance drops from 2.875 to 1.496 Å for the

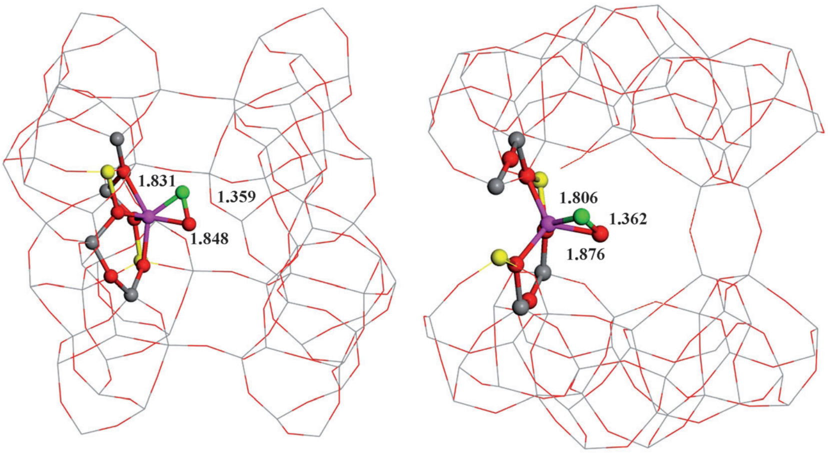

Figure 4. Optimized structure of complex **11** [α model (left) and β−2 model (right)]. The distances are in Å. Silicon atoms are in gray, aluminum atoms in yellow, iron atoms in violet, and oxygen atoms in red; the O_{EXFR} atom is shown in green.

© 2013 Wiley-VCH Verlag GmbH & Co. KGaA, Weinheim

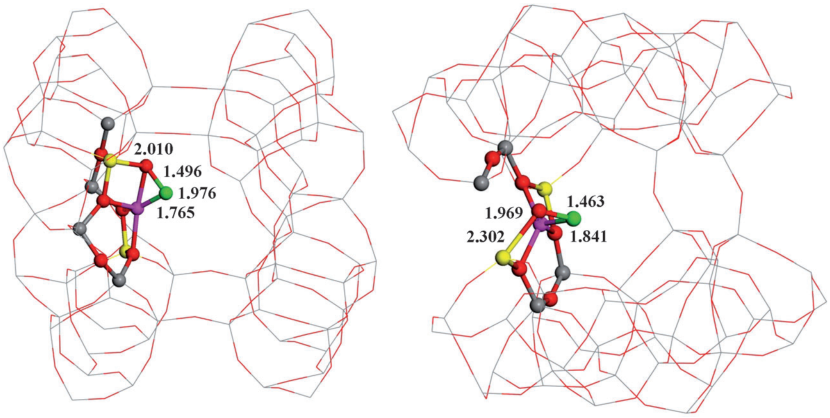

Figure 5. Optimized structure of transition states **TS5** and **TS6** [α model (left) and β−2 model (right)]. The distances are in Å. Silicon atoms are in gray, aluminum atoms in yellow, iron atoms in violet, and oxygen atoms in red; the O_{EXFR} atom is shown in green.

α site and from 2.986 to 1.463 Å for the β−2 site when transition state **TS5** is formed. This distance further decreases to 1.359 and 1.362 Å for the α and β−2 sites, respectively, to yield complex **11** with a unique structural feature which is the $-^{16}O-^{18}O-$ fragment above the plane of the cationic site and an oxygen vacancy created in the cationic site (Figure 4). The formation of complex **11** is calculated to be extremely endothermic, 104.2 and 116.1 kcal mol^{-1} for the α and β−2 sites, respectively. The calculated barrier is prohibitively high as its value reaches 109.3 and 136.7 kcal mol^{-1} for the α and β−2 sites, respectively. This reaction step is rate determining for the isotope exchange between O_{EXFR} and O_{FR} in the absence of O_2 molecules. The presence of the $-^{16}O-^{18}O-$ fragment and the oxygen vacancy enables the oxygen exchange to occur since ^{18}O can occupy the oxygen vacancy in the cationic site to yield complex **12** via transition state **TS6** (the reaction energies are −104.2 and −116.1 kcal mol^{-1} for the α and β−2 sites, respectively, and the energy barriers are 5.1 and 20.6 kcal mol^{-1} for the α and β−2 sites, respectively).

3.2.4. Mechanism of the Isotope Exchange between O_{EXFR} and O_{FR} in the Presence of O_2 Molecules

Calculations performed on the α and β−2 models reveal that the presence of O_2 molecules significantly facilitates the isotope exchange between O_{EXFR} and O_{FR}. As reported in section 3.2.2, complex **6** reacts with $^{16}O_2$ to yield complex **8** (Scheme 2). A possibility that is addressed here is (Scheme 4) that the $^{16}O-^{16}O$ bond in the $-^{16}O-^{16}O-^{18}O-$ fragment in complex **8** breaks and ^{16}O forms a bond with one of the four O_{FR} atoms to give complex **13** (Figure 6) via transition state **TS7** (Figure 7). The calculated reaction energies are 20.5 (α) and 25.7 kcal mol^{-1} (β−2), and the corresponding barriers are 24.9 (α) and 27.2 kcal mol^{-1}

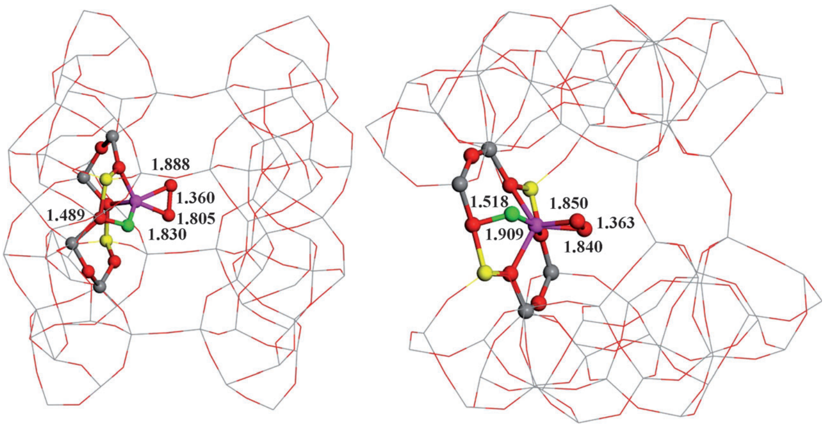

Figure 6. Optimized structure of complex **13** [α model (left) and β−2 model (right)]. The distances are in Å. Silicon atoms are in gray, aluminum atoms in yellow, iron atoms in violet, and oxygen atoms in red; the O_{EXFR} atom is shown in green.

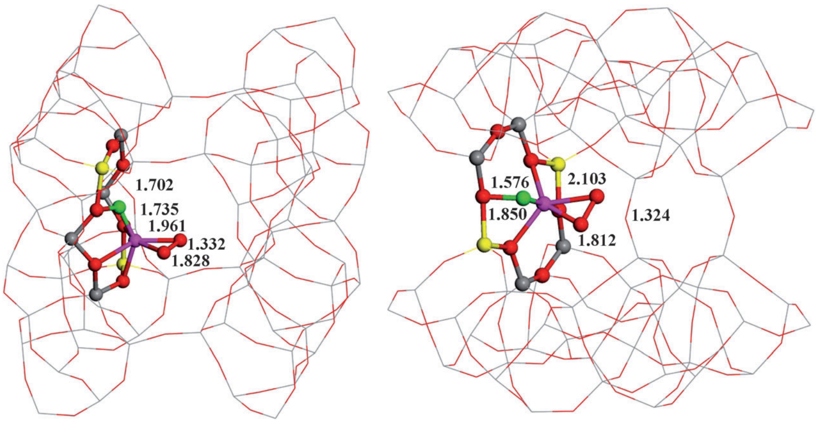

Figure 7. Optimized structure of the transition state **TS7** [α model (left) and β−2 model (right)]. The distances are in Å. Silicon atoms are in gray, aluminum atoms in yellow, iron atoms in violet, and oxygen atoms in red; the O_{EXFR} atom is shown in green.

© 2013 Wiley-VCH Verlag GmbH & Co. KGaA, Weinheim

(β−2). The corresponding ^{16}O–^{16}O distance decreases from 2.826 and 2.767 Å in **8** to 1.702 and 1.576 Å in **TS7** and further to 1.489 and 1.518 Å in **13**, respectively. The –^{16}O–^{18}O– fragment above the plane of the cationic site which is the key structural feature of complex **11** (Scheme 3) is already formed in **13**. Therefore, the newly formed $^{16}O_2$ molecule is released from complex **13** to the gas phase and complex **11** is formed. This reaction step is calculated to be very endothermic as the reaction energies are 87.9 and 87.3 kcal mol^{-1} for the α and β−2 sites, respectively. There was no transition state found for this reaction step, thus the corresponding reaction energy indicates that it is the rate-determining step of the isotope exchange between O_{EXFR} and O_{FR} in the presence of O_2. Since the O_2 molecule is released to the gas phase, this reaction step is irreversible. Therefore complex **11** cannot rearrange back to yield complex **13** despite the absence of a calculated barrier separating **11** and **13**, as all our attempts to locate a transition state connecting **11** and **13** were unsuccessful. Furthermore, O_2 from the gas phase cannot adsorb later on Fe in **11** to yield back **13** since complex **11** quickly rearranges to form complex **12** (see Section 3.2.3).

4. Discussion

Using ^{18}O-labeled compounds allows for the examination of the mechanism of the N_2O decomposition by analyzing the isotope composition of either the solid catalyst or, more effectively, the gas phase (O_2). Our results indicate that there is no isotope exchange between unreacted nitrous oxide and ferrierite in our experiments, since no $N_2{}^{16}O$ is observed. Thus, the presence of ^{16}O in O_2 indicates the isotope exchange of $^{18}O_{EXFR}$ with the $^{16}O_{FR}$ atoms which form the active site since the $Fe_{0.04}$-FER sample used contains exclusively Fe^{II} accommodated in the α and β cationic sites due to the very low Fe/Al ratio.[10] There are no other iron species (e.g. iron oxides) present in $Fe_{0.04}$-FER.[10] The number of participating framework oxygen atoms in the isotope exchange can be determined from the concentration of ^{16}O in the released O_2 molecules because all ^{16}O atoms exclusively originate from the zeolite framework.

An Fe^{II} cation is coordinated to the four oxygen atoms, forming the cationic site.[7] After the Fe^{II} in the fresh $Fe((^{16}O_{FR})_4)$-FER sample is oxidized by $N_2{}^{18}O$ to give $^{18}O_{EXFR}{=}Fe((^{16}O_{FR})_4)$-FER, the isotope exchange can occur. We assume that in the temperature interval of our experiments, $^{18}O_{EXFR}$ exchanges with one of the four O_{FR} atoms to yield $^{16}O_{EXFR}{=}Fe((^{16}O_{FR})_3{}^{18}O_{FR})$-FER. These four Fe framework oxygen atoms, $^{16}O_{FR}$, are the closest to Fe extra-framework oxygen atoms, $^{18}O_{EXFR}$, and they can directly exchange with $^{18}O_{EXFR}$. All other framework oxygen atoms, $^{16}O_{FR}$, besides the four forming the cationic site are too distant from the Fe extra-framework oxygen atoms, $^{18}O_{EXFR}$, and we presume that in the studied temperature range they cannot directly exchange with $^{18}O_{EXFR}$. This assumption is consistent with the observed values of O_{exch}/Fe which under the conditions used in this study never exceed four. This reasoning is further supported by the experimental evidence showing that there is no isotope exchange observed in the absence of Fe in the ferrierite sample indicating the necessity of the presence of a metal center. In addition, we observed no equilibration of a mixture of $^{18}O_2$ and $^{16}O_2$ without the presence of N_2O (i.e. in the absence of O_{EXFR}), revealing that the isotope exchange occurs exclusively in the Fe^{II} cationic sites. The isotope exchange proceeds further and O_{EXFR} atoms exchange again with one of the four O_{FR} atoms forming the cationic site.

There are only three nitrous oxide molecules per one Fe cation in the beginning of our batch experiments, therefore N_2O is decomposed to N_2(g) and O_2(g) on only a small part of the active sites formed by two cooperating Fe cations in two adjacent β sites of Fe-ferrierite.[7] In such a case, surface NO_x species are formed (four N_2O molecules are needed to give $Fe(O_4)NO_3$-FER) and the N_2O decomposition proceeds via $Fe(O_4)NO_x$-FER.[22] The remaining active sites with two cooperating Fe cations without the presence of adsorbed NO_x do not efficiently catalyze the N_2O decomposition, because no surface NO_x species are formed at these sites. On the other hand, these Fe structures are easily oxidized[7] by N_2O and then the isotope exchange of both O_{EXFR} with O_{FR}, as well as O_{EXFR} with O_2 molecules, occurs. Cationic sites with isolated Fe cations can be also oxidized,[7] and so they contribute to the isotope exchange. Some sites with isolated Fe cations can be blocked in the initial stages of the N_2O decomposition due to the formation of the Fe···NNO complex.[7] Therefore, we conclude that during the N_2O decomposition on Fe-FER most Fe cations are oxidized, a small part of Fe form surface NOx species, and the remaining Fe cations either create the Fe···NNO complex or are eventually empty.

Panov et al. showed that the process of the isotope exchange with O_2 molecules occurs even at room temperature[6e] and yields equilibrated oxygen isotopologues.[23] The *Q* variable attains the value of four in the whole temperature range (Figure 1), revealing that the equilibrium among the isotopologues of O_2 molecules is reached for all the temperatures. Our calculated value of the activation energy of the rate-determining step of the isotope exchange between O_{EXFR} and O_2 molecules (Schemes 1 and 2) is consistent with the observed facile occurrence of the isotope exchange with O_2 molecules.

The detailed mechanism of the recombination of two O_{EXFR} atoms to give an O_2 molecule which proceeds mainly via $Fe(O_4)NO_x$-FER is beyond the scope of this study. When the N_2O_{decomp}/Fe ratio is one and two, then the concentration of ^{18}O in the released O_2 molecules is 20 and 30 %, respectively, at full equilibration between O_{EXFR} and O_{FR} atoms (see the SI for details). Conversely, when there is no isotope exchange between O_{EXFR} and O_{FR} atoms, the concentration of ^{18}O in the formed O_2 molecules is 100 % regardless of the number of decomposed N_2O molecules per Fe. Table 1 shows that the measured N_2O_{decomp}/Fe values are 1.6, 2.6, and 2.9 at 553, 573, and 593 K, respectively. Therefore, the concentration of ^{18}O in the released O_2 molecules is estimated to be 28, 37, and 39 % (see the SI for details) at 553, 573, and 593 K if there is a full equilibration between O_{EXFR} and O_{FR} atoms at all Fe cationic sites. However, the observed concentration of ^{18}O in the released O_2 molecules formed on Fe-FER after 40 min is higher, approximately 55 % at 553 K, 50 % at 573 K, and 45 % at 593 K (Figure 1) indicating that O_{EXFR} atoms are not fully equilibrated

© 2013 Wiley-VCH Verlag GmbH & Co. KGaA, Weinheim

with O_{FR} atoms at 553 and 573 K, while at 593 K the equilibrium is almost reached after 40 min. These experimental results show that the oxygen exchange is more sluggish than the N_2O decomposition.

Our DFT calculations reveal that the energy cost of a creation of an oxygen vacancy starting from the ferrierite framework without structural defects is prohibitively high as the reaction barrier reaches 109.3 and 136.7 kcal mol^{-1} for the α and $\beta-2$ sites, respectively (Scheme 3). Therefore, other possible routes of oxygen exchange were investigated to rationalize the observed framework-oxygen mobility. We discovered that O_2 molecules originating from the decomposing N_2O significantly facilitate the isotope exchange (Scheme 4). The easiest mechanism of oxygen exchange involves complex **8**, which is formed from complex **6** and O_2 (Scheme 2). Our computational results reveal that the energy cost of the rate-determining step of the isotope exchange between O_{EXFR} and O_{FR} in the presence of O_2 drops to 87.9 and 87.3 kcal mol^{-1} (Scheme 4) for the α and $\beta-2$ sites, respectively. These values are still very high since the mechanism of the isotope exchange involves the formation of a defect in the cationic site (complex **11**). The creation of the defect includes a cleavage of covalent bonds, and therefore, complex **11** with an oxygen vacancy is very high in energy. Since a molecule of O_2 is released into the gas phase, the formation of complex **11** is entropically favored resulting into a slightly lower free energy barrier of the rate-determining step of the isotope exchange.

We presume that the calculated energy barrier of 87 kcal mol^{-1} (Scheme 4) is higher than the assumed experimental value since otherwise the oxygen exchange would be extremely sluggish to occur at 553 K. The reason of the overestimation of the calculated value is most likely the fact that our computational model considers the ideal Fe^{II} exchanged ferrierite without structural defects. The only source of ^{16}O in the O_2 molecules formed by the $N_2{}^{18}O$ decomposition over our $Fe_{0.04}$-FER sample is framework ^{16}O atoms as there are no other species containing ^{16}O in the sample. However, the zeolite sample used was not completely free of defects. The oxygen exchange requires a formation of an oxygen vacancy in the Fe site or the presence of a preexisting structural defect in the vicinity of the Fe site. In the confines of the computational model and the absence of reliable data regarding the defects, we can only model the simplest of defects, that is, a framework oxygen vacancy (Scheme 3). Our computational results for the defect-free zeolite framework (Scheme 4) are the upper bound of the corresponding reaction barriers of the exchange between O_{EXFR} and O_{FR}. Preexisting structural defects in the vicinity of the Fe site in the catalyst are likely responsible for the more facile occurrence of the oxygen exchange than suggested by our DFT calculations.

The formation of complex **8** (Figure 3) featuring an –O–O–O– fragment bound to the Fe^{II} cation by both the terminal O atoms from the Fe-O complex and O_2 (Scheme 2) indicates that the structure of the active sites of catalysts based on Fe^{II}-exchanged zeolites is in reality complex, and the Fe-O_{EXFR} structure presents a simplification of the real active site. The possible presence of various arrangements of atoms in the active sites of iron-exchanged zeolites likely affects their catalytic activity. We presume that in the real catalyst, under the reaction conditions, there might also exist another structural variant of the active site (i.e. a complex similar to complex **8**), especially when a possible presence of pre-existing structural defects in the vicinity of the Fe site is considered, for which the isotope exchange is more facile than that for complex **8** (Scheme 4). However, we were not able to localize any such complex on the potential energy surface using our model without structural defects.

5. Conclusions

The occurrence of an isotope exchange indicates that zeolite-framework O atoms are involved in the formation of O_2 molecules during the N_2O decomposition catalyzed by Fe-ferrierite. Our combined experimental and theoretical investigation of the role of O_{FR} atoms of Fe^{II}-exchanged ferrierites in the N_2O decomposition shows plausible mechanisms of the isotope exchange between the O_{EXFR} atoms and the O_{FR} atoms. Our results in the temperature interval from 553 to 593 K are consistent with the mobility limited to the four O_{FR} atoms forming cationic sites accommodating Fe. Our DFT calculations reveal that O_2 molecules facilitate the oxygen exchange. However, the corresponding calculated energy barrier of 87 kcal mol^{-1} is still very high, and it is higher than the assumed experimental value based on the occurrence of the sluggish oxygen exchange at 553 K. Most likely, the presence of defects in the real zeolite catalyst is responsible for the more facile occurrence of oxygen exchange compared to what was suggested by our DFT calculations.

Acknowledgements

This study was performed with institutional support RVO:61388955 and was further supported by the Grant Agency of the Academy of Sciences of the Czech Republic (Project # IAA400400812) and the Grant Agency of the Czech Republic (Project # GA 203/09/1627).

Keywords: density functional theory · iron · isotopes · mass spectrometry · zeolites

[1] a) Y. Traa, B. Burger, J. Weitkamp, *Microporous Mesoporous Mater.* **1999**, *30*, 3–41; b) B. Wichtelova, Z. Sobalik, J. Dedecek, *Appl. Catal. B* **2003**, *41*, 97–114.

[2] a) G. I. Panov, V. I. Sobolev, A. S. Kharitonov, *J. Mol. Catal.* **1990**, *61*, 85–97; b) K. A. Dubkov, N. S. Ovanesyan, A. A. Shteinman, E. V. Starokon, G. I. Panov, *J. Catal.* **2002**, *207*, 341–352; c) J. Perez-Ramirez, *J. Catal.* **2004**, *227*, 512–522; d) J. Perez-Ramirez, J. C. Groen, A. Bruckner, M. S. Kumar, U. Bentrup, M. N. Debbagh, L. A. Villaescusa, *J. Catal.* **2005**, *232*, 318–334; e) K. Jisa, J. Novakova, M. Schwarze, A. Vondrova, S. Sklenak, Z. Sobalik, *J. Catal.* **2009**, *262*, 27–34; f) Z. Sobalik, J. Novakova, J. Dedecek, N. K. Sathu, E. Tabor, P. Sazama, P. Stastny, B. Wichterlova, *Microporous Mesoporous Mater.* **2011**, *146*, 172–183; g) J. Dedecek, L. Capek, P. Sazama, Z. Sobalik, B. Wichterlova, *Appl. Catal. A* **2011**, *391*, 244–253; h) E. Tabor, K. Zaveta, N. K. Sathu, A. Vondrova, P. Sazama, Z. Sobalik, *Catal. Today* **2011**, *175*, 238–244.

© 2013 Wiley-VCH Verlag GmbH & Co. KGaA, Weinheim

[3] a) G. I. Panov, A. S. Kharitonov, V. I. Sobolev, *Appl. Catal. A* **1993**, *98*, 1–20; b) D. P. Ivanov, M. A. Rodkin, K. A. Dubkov, A. S. Kharitonov, G. I. Panov, *Kinet. Catal.* **2000**, *41*, 771–775; c) L. Capek, P. Kubanek, B. Wichterlova, Z. Sobalik, *Collect. Czech. Chem. Commun.* **2003**, *68*, 1805–1818; d) J. Perez-Ramirez, A. Gallardo-Llamas, *Appl. Catal. A* **2005**, *279*, 117–123.

[4] a) Z. Sobalik, A. Vondrova, Z. Tvaruzkova, B. Wichterlova, *Catal. Today* **2002**, *75*, 347–351; b) R. Brosius, D. Habermacher, J. A. Martens, L. Vradman, M. Herskowitz, L. Capek, Z. Sobalik, J. Dedecek, B. Wichterlova, V. Tokarova, O. Gonsiorova, *Top. Catal.* **2004**, *30–1*, 333–339; c) L. Capek, L. Vradman, P. Sazama, M. Herskowitz, B. Wichterlova, R. Zukerman, R. Brosius, J. A. Martens, *Appl. Catal. B* **2007**, *70*, 53–57; d) M. Iwasaki, K. Yamazaki, K. Banno, H. Shinjoh, *J. Catal.* **2008**, *260*, 205–216; e) D. E. Doronkin, A. Y. Stakheev, A. V. Kucherov, N. N. Tolkachev, M. Kustova, M. Hoj, G. N. Baeva, G. O. Bragina, P. Gabrielsson, I. Gekas, S. Dahl, *Top. Catal.* **2009**, *52*, 1728–1733; f) M. Colombo, I. Nova, E. Tronconi, *Catal. Today* **2010**, *151*, 223–230; g) J. H. Li, H. Z. Chang, L. Ma, J. M. Hao, R. T. Yang, *Catal. Today* **2011**, *175*, 147–156; h) M. P. Ruggeri, A. Grossale, I. Nova, E. Tronconi, H. Jirglova, Z. Sobalik, *Catal. Today* **2012**, *184*, 107–114.

[5] a) E. R. S. Winter, *Adv. Catal.* **1958**, *10*, 196–241; b) E. R. S. Winter, *J. Catal.* **1974**, *34*, 431–439.

[6] a) J. Leglise, J. O. Petunchi, W. K. Hall, *J. Catal.* **1984**, *86*, 392–399; b) J. Valyon, W. S. Millman, W. K. Hall, *Catal. Lett.* **1994**, *24*, 215–225; c) G. D. Pirngruber, P. K. Roy, *Catal. Lett.* **2004**, *93*, 75–80; d) G. D. Pirngruber, P. K. Roy, R. Prins, *J. Catal.* **2007**, *246*, 147–157; e) M. V. Parfenov, E. V. Starokon, S. V. Semikolenov, G. I. Panov, *J. Catal.* **2009**, *263*, 173–180; f) J. Nováková, M. Lhotka, Z. Tvaruzkova, Z. Sobalik, *Catal. Lett.* **2002**, *83*, 215–220; g) J. Nováková, M. Schwarze, Z. Sobalik, *Catal. Lett.* **2005**, *104*, 157–162; h) Y. F. Chang, G. A. Somorjai, H. Heinemann, *J. Catal.* **1995**, *154*, 24–32; i) J. F. Jia, B. Wen, W. M. H. Sachtler, *J. Catal.* **2002**, *210*, 453–459; j) J. Nováková, Z. Sobalik, *Catal. Lett.* **2009**, *131*, 530–537; k) E. V. Starokon, M. V. Parfenov, S. E. Malykhin, G. I. Panov, *J. Phys. Chem. C* **2011**, *115*, 12554–12559.

[7] S. Sklenak, P. C. Andrikopoulos, B. Boekfa, B. Jansang, J. Novakova, L. Benco, T. Bucko, J. Hafner, J. Dedecek, Z. Sobalik, *J. Catal.* **2010**, *272*, 262–274.

[8] CZ 293917 B6 **2001**.

[9] J. Dedecek, M. J. Lucero, C. B. Li, F. Gao, P. Klein, M. Urbanova, Z. Tvaruzkova, P. Sazama, S. Sklenak, *J. Phys. Chem. C* **2011**, *115*, 11056–11064.

[10] E. Tabor, K. Zaveta, N. K. Sathu, Z. Tvaruzkova, Z. Sobalik, *Catal. Today* **2011**, *169*, 16–23.

[11] a) G. Kresse, J. Furthmuller, *Phys. Rev. B* **1996**, *54*, 11169–11186; b) G. Kresse, J. Furthmuller, *Comput. Mater. Sci.* **1996**, *6*, 15–50; c) G. Kresse, J. Hafner, *Phys. Rev. B* **1993**, *48*, 13115–13118; d) G. Kresse, J. Hafner, *Phys. Rev. B* **1994**, *49*, 14251–14269.

[12] a) L. Benco, T. Bucko, R. Grybos, J. Hafner, Z. Sobalik, J. Dedecek, J. Hrusak, *J. Phys. Chem. C* **2007**, *111*, 586–595; b) L. Benco, T. Bucko, R. Grybos, J. Hafner, Z. Sobalik, J. Dedecek, S. Sklenak, J. Hrusak, *J. Phys. Chem. C* **2007**, *111*, 9393–9402.

[13] P. E. Blöchl, *Phys. Rev. B* **1994**, *50*, 17953–17979.

[14] G. Kresse, D. Joubert, *Phys. Rev. B* **1999**, *59*, 1758–1775.

[15] a) J. P. Perdew, J. A. Chevary, S. H. Vosko, K. A. Jackson, M. R. Pederson, D. J. Singh, C. Fiolhais, *Phys. Rev. B* **1992**, *46*, 6671–6687; b) J. P. Perdew, Y. Wang, *Phys. Rev. B* **1992**, *45*, 13244–13249.

[16] G. Henkelman, H. Jonsson, *J. Chem. Phys.* **1999**, *111*, 7010–7022.

[17] A. Heyden, A. T. Bell, F. J. Keil, *J. Chem. Phys.* **2005**, *123*, 224101.

[18] D. A. McQuarrie, *Statistical Thermodynamics*, University Science Books, Mill Valley, CA, **1973**.

[19] J. L. Carreón-Macedo, J. N. Harvey, *Phys. Chem. Chem. Phys.* **2006**, *8*, 93–100.

[20] H. Guesmi, D. Berthomieu, L. Kiwi-Minsker, *J. Phys. Chem. C* **2008**, *112*, 20319–20328.

[21] a) J. N. Harvey, M. Aschi, *Phys. Chem. Chem. Phys.* **1999**, *1*, 5555–5563; b) J. N. Harvey, M. Aschi, H. Schwarz, W. Koch, *Theor. Chem. Acc.* **1998**, *99*, 95–99.

[22] J. Nováková, Z. Sobalik, *Catal. Lett.* **2006**, *111*, 195–202.

[23] K. Klier, J. Novakova, P. Jiru, *J. Catal.* **1963**, *2*, 479–484.

Received: November 1, 2012
Published online on January 14, 2013

© 2013 Wiley-VCH Verlag GmbH & Co. KGaA, Weinheim